Identification of the material parameters of an aortic wall

Autor: Lukáš Horný[1], Rudolf Žitný[2], Hynek Chlup[1], Hana Macková[1]

[1] Department of Mechanics, Biomechanics and Mechatronics, Faculty of Mechanical Engineering, CTU in Prague, Technická 4, 166 07, Praha 6, Czech Republic
[2] Department of Process Engineering, Faculty of Mechanical Engineering, CTU in Prague, Technická 4, 166 07, Praha 6, Czech Republic
<lukas.horny@fs.cvut.cz>

Abstract

The passive mechanical response of arterial walls continues to be a topic of great interest. Inflation tests with human thoracic aorta specimens were performed with the aim of fitting a material model. The experimental data was used in a nonlinear regression analysis to identify the material parameters. The aortic tissue was assumed to be an incompressible hyperelastic material. We used a 5–parameter strain energy density function based on a combination of an isotropic Neo–Hookean expression and a Fung–type orthotropic expression. The computational model for identifying the material parameters was based on the boundary value problem of an inflated thick–walled tube with axial pre–strains. The circumferential residual strains were included. The internal structure of the arterial walls was not considered. The fitted material models correspond very well with the experimental data. Significant stiffening under large strains was observed. It was concluded that the combined model of the strain energy density function is suitable for the aortic mechanical response description. The material parameters satisfy the convexity conditions.

Keywords: aorta, constitutive modeling, fung-type model, inflation test, hyperelasticity, neo-Hookean model.

1 Introduction

The mechanical behavior and constitutive modeling of arterial walls continues to be a topic of great interest. The constitutive equations are needed in every computational model and in developing modern treatment techniques. The most frequent approach for obtaining the constitutive

relations is based on the assumption of hyperelasticity of the arterial wall. Many forms of the strain energy density function determining the constitutive relations have been proposed in the last thirty years. The most successful of these are based on an exponential expression of the functional dependence between stored energy and strain. These types of strain energy functions are derived from the functional form originally proposed by Fung et al [1]. A detailed review of frequently used strain energy functions can be found in Holzapfel, Gasser and Ogden [2]. Here we see that the latest constitutive models take into account the composite structure of the arterial wall. Great attention is being paid to collagen fiber reinforcement, see, e.g., the studies published by Gasser, Ogden and Holzapfel [3] and by Zulliger et al [4]. In recent years a structural approach has received much greater attention in arterial wall biomechanics. This is also shown by the growing number of layered models that take arterial wall layers into account. The number of studies where the arterial wall is modeled as a layered structure continues to increase, see [5], [6], [7] and more recent papers [2], [8] and [9]. Especially we would like to mention here the most recent paper published by Holzapfel [10], where the same constitutive model is used to identify the material parameters of arterial layers by means of uniaxial extension tests. In spite of the increasing number of structurally motivated investigations, there is still only a limited amount of structural data based on experiments. Generally, however, extending the experimental data on arterial passive mechanical responses is still of importance. Our study therefore aims to investigate the passive mechanical response of the human aorta, and to identify its material parameters.

2 Methods

Inflation and uni–axial extension tests were performed with specimens of human thoracic aorta in order to fit the material model. Tissue from a 47-year-old female (F47) and from a 54-year-old male (M54) was obtained during autopsies at the Institute of Forensic Medicine of the University Hospital Na Kralovskych Vinohradech in Prague. No significant atherosclerotic changes were found. The time between the presumptive death and the inflation tests was 50 hours in the case of F47 and 66 hours for M54. The specimens were moved back to the Institute of Forensic Medicine after the experiments for ethical disposal. In our paper, the aortic wall is modeled phenomenologically as a homogeneous structure, because histological analyses were not available when the measurements were made.

The arterial wall was considered as an incompressible, orthotropic and hyperelastic material. The selected type of strain energy density function was in the form published by Weizsäcker and Holzapfel in [11] and [12]. This kind of strain energy density function comprises a Neo-Hookean isotropic part related to the initial state of deformation and a Fung-type orthotropic part related to large strains:

$$\psi = \psi_{iso} + \psi_{aniso} = c_1 \left(I_1 - 3\right) + c_2 \left(e^{b_1 E_{tt}^2 + b_2 E_{zz}^2 + 2b_3 E_{tt} E_{zz}} - 1\right) \tag{1}$$

Here c_1, c_2, b_1, b_2 and b_3 are material parameters. The first invariant of a right Cauchy–Green strain tensor is denoted I_1, and E_{ii} means components of the Green strain tensor. The reference coordinate system is cylindrical, and axes t, z and r coincide with the circumferential, axial and radial direction, respectively. This is a phenomenological type of strain energy density function, but some structural aspects are also considered here. The neo-Hookean part represents the energy stored in non-collagenous components of the wall (e.g. elastin, smooth muscle cells and proteoglycans). The energy stored in the non-collagenous matrix of the arterial wall composite is related mainly to the low strain domain. On the other hand, the Fung-type part of the strain energy function is related to stiffening under large strains, which is assumed to be related to elongation of the collagenous fibers. At first, the collagenous fibers are undulated, and under

large strains they are elongated and then, due to the high fiber stiffness, exponential arterial wall stiffening is observed; more information can be found in Roach and Burton [15] or in Hayashi [16]. For further details about the model used here, see papers published by Holzapfel and Weizsäcker [12] and Holzapfel [10]. Holzapfel and Weizsäcker [12] used the same type of strain energy function to identify the material parameters of a rat abdominal aorta and a tail artery. Carboni et al. [13] used this model for a porcine coronary left circumflex artery, and Schulze-Bauer [14] used it for human iliac arteries. Model (1) has not been used before for a human thoracic aorta, to the best of the authors' knowledge.

I_1 can be expressed in the following form:

$$I_1 = \lambda_t^2 + \lambda_z^2 + \lambda_r^2 \tag{2}$$

Here, λ_i are stretch ratios in the circumferential, axial and radial direction. An arterial segment is modeled as a thick-walled tube in the inflation test. Under the kinematics of a thick-walled tube, the stretch ratios can be expressed as follows:

$$\begin{aligned} \lambda_t &= \frac{\pi\ r}{\theta\ R^*} \\ \lambda_z &= \frac{l}{L} \\ \lambda_r &= \frac{\partial r}{\partial R^*} \end{aligned} \tag{3}$$

The circumferential stretch ratio λ_t is obtained as the ratio of the reference circumference to the current circumference. The current configuration (an inflated and axially pre-strained artery) is cylindrical, but the reference configuration of an unloaded artery is obtained after a radial cut of the arterial segment. Due to the presence of circumferential residual strains, the artery will open up into a partial cylinder. This partial cylinder is characterized by the opening angle α ($\theta = \pi - \alpha$), which is a measure of the residual strains. Hence, the reference circumference is obtained as θR^*. Here R^* is the reference radius. The current radius in (3a) is denoted as r. Hence residual strains are included in the computational model. A detailed study of the residual strains in arteries can be found in Rachev and Greenwald [17]. The entire situation is illustrated in Fig. 1. The axial stretch ratio λ_z in (3b) is obtained as the ratio of the current length, l, to the reference length, L. The radial stretch ratio, λ_r, as a component of the deformation gradient, can be expressed as a derivative of the spatial coordinate with respect to the reference ratio, (3c). However, we adopted the incompressibility condition, which is generally used when a soft tissue is modeled. Thus, λ_r can be obtained as a combination of the circumferential and axial stretch ratios:

$$\lambda_t \lambda_z \lambda_r = 1 \tag{4}$$

The stretch ratios can be transformed into Green strains, as follows:

$$E_{ii} = \frac{1}{2}(\lambda_i^2 - 1) \qquad i = t, z, r \tag{5}$$

The local stress – strain relationships in a hyperelastic continuum are given by the derivatives of the strain energy density function ψ with respect to the Green strain tensor components:

$$\sigma_{ii} = -p + \lambda_i^2 \frac{\partial \psi}{\partial E_{ii}} \qquad i = t, z, r \tag{6}$$

Here σ_{ii} are components of the Cauchy stress tensor, λ_i are stretch ratios and p is the unknown hydrostatic pressure that must be determined through a boundary condition. The presence of shear stresses and strains is not considered, in accordance with (3) and (6). The stress – strain relationship will be obtained after differentiation in (6), and will be rewritten in kinematic terms.

The resultant expressions still contain the unknown material parameters c_1,c_2, b_1, b_2 and b_3 that occur in (1). The aim of our study is to find their numerical values. The boundary condition of a thick-walled tube can be used for this purpose.

A thick-walled tube must satisfy radial force equilibrium. An equation for the radial equilibrium of a thick-walled tube is:

$$\frac{\mathrm{d}\sigma_r}{\mathrm{d}r} + \frac{\sigma_{rr} - \sigma_{tt}}{r} = 0 \tag{7}$$

and the boundary condition at inner radius r_i must be satisfied:

$$\sigma_{rr}(r_i) = -p \tag{8}$$

There is also a second boundary condition on the outer radius, where the pressure and the radial stress are assumed to be zero. Denotations used in equations (7) and (8): σ_{rr} radial Cauchy stress; σ_{tt} – circumferential Cauchy stress; r – deformed radius; r_i – deformed inner radius. When the incompressibility condition is considered (4), there are only two independent stretch ratios. The increment of the strain energy when there is a deformation is given as:

$$\mathrm{d}\psi = \lambda_r\lambda_t\sigma_{zz}\mathrm{d}\lambda_z + \lambda_r\lambda_z\sigma_{tt}\mathrm{d}\lambda_t + \lambda_t\lambda_z\sigma_{rr}\mathrm{d}\lambda_r \tag{9}$$

When we express (9) taking into account (4) and differentiate (4) and compare back with (9), we will obtain:

$$\sigma_{tt} - \sigma_{rr} = \lambda_i^2 \frac{\partial\psi}{\partial E_{tt}} \tag{10}$$

Integration of (7) through the arterial wall and the boundary condition gives:

$$\sigma_{rr}\,(r_i) = \int_{r_i}^{r_o} \frac{\sigma_{tt} - \sigma_{rr}}{r} dr \tag{11}$$

Substituting (10) into (11) gives:

$$\sigma_{rr}\,(r_i) = \int_{r_i}^{r_o} \lambda_t^2 \frac{\partial\psi}{\partial E_{tt}} \frac{dr}{r} \tag{12}$$

The denotation through (9) to (12) corresponds to that used above. Equation (12) is fundamental to our analysis. It can be integrated numerically and the value of the radial stress is determined. This provides a method for identifying the material parameters that remain in the derivative of ψ. Two things need to be mentioned here. First, the radial equilibrium equation is essentially related to the thick–walled computational model of the artery. Second, it is clear that the incompressibility condition is also essential, and the strain energy density function in (1) takes this into account. This is the case when the three dimensional state of the stress is predicted with a two-dimensional strain energy density function. The limitations and possibilities of a two–dimensional formulation of the strain energy density function are discussed, e.g., in [2].

Hence, equation (12) can be used in a regression analysis of the experimental data. The following section will describe experiments in which an artery is inflated and axially prestrained, and the outer radius, axial prestrains and internal pressure are measured. After this data has been obtained, regression analysis can be performed according to (13), as follows.

$$\frac{\partial}{\partial a_k} \sum_{j=1}^{n} \left(\sigma_{rr}\,(r_{ij}, \lambda_t, \lambda_z, a_1, .., a_5) - p_{ij}\right)^2 = 0 \qquad k = 1, \ldots, 5 \tag{13}$$

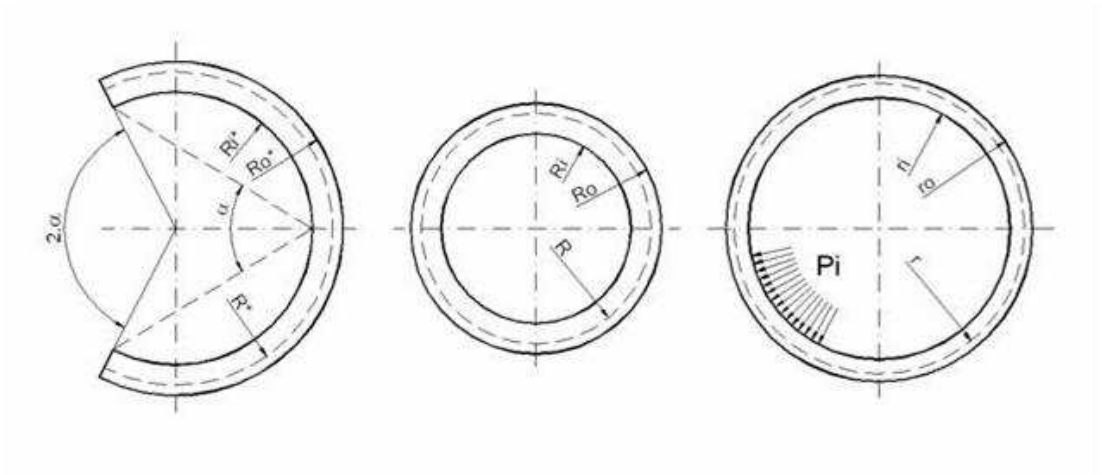

Figure 1: Deformation states of an artery. Left side – an opened segment (zero stress state, reference state); middle – a closed segment; right – loaded state (spatial configuration).

The standard least squares method was used in our study, and the numerical values of the material parameters were found, using the Levenberg–Marquardt method to solve the nonlinear regression equations. The material parameters in (13) are now denoted $a_1, \ldots$. In equation (13), p_i means the internal pressure when j is measured. Finally, it should be noted that the inner radius is obtained taking into account the incompressibility condition and comparing the volumes in the reference (zero stress) configuration and the spatial (loaded) configuration. A similar approach to identifying the material parameters in the constitutive equation, based on a thick-walled tube with residual strains, can be found in Matsumoto and Hayashi [18].

3 Experiments

The inflation experiments were performed using a pressure – diameter experimental device that was developed in our laboratory. This apparatus includes a pressure generator, two pressure probes to control the internal pressure, an optical system to measure the outer radius, and an adjustable system for fixing the specimen. Different values of the axial pre–strain can be set up using this apparatus. The whole experimental system is documented in Figure 2. The outer diameter was recorded using a digital camera, and an accurate value for the diameter was determined via an image analysis. An injection was used as the pressure generator, and was operated manually. All measurements were static, with a step change of the internal pressure and fixed axial pre–strain.

The inflation experiments were performed under the following conditions. A tubular sample of F47 was subjected to four pressurization cycles in the pressure range 0 kPa – 28 kPa – 0 kPa under axial pre–stretch $\lambda_z = 1.32$ and four cycles in the pressure range 0 kPa – 28 kPa – 0 kPa under $\lambda_z = 1.4$, respectively. In the case of M54, there were 6 cycles in the range 0 kPa – 18 kPa – 0 kPa under $\lambda_z = 1.3$ and 3 cycles in the pressure range 0 kPa – 20 kPa – 0 kPa under $\lambda_z = 1.42$, respectively. The opening angles were measured after a radial cut of specially prepared rings of the arteries before pressurization. All experiments were performed at room temperature and the specimens were stored at a temperature approximately of 4°C.

It should to be noted that arteries are not ideally cylindrical and their walls include places where the cylindrical shape is affected by branching. The specimens used in our study were obtained from the thoracic aorta, which includes a few pairs of fine costal arteries. These were cut, but

Parameters **Dimension**	c_1 [kPa]	c_2 [kPa]	b_1 [1]	b_2 [1]	b_3 [1]	I^2 [1]
F47	27.55	0.3133	25	5.869	0.9391	0.96
M54	25.76	0.9315	7.985	6.566	0.3101	0.97

Table 2: Summary of the identified material parameters

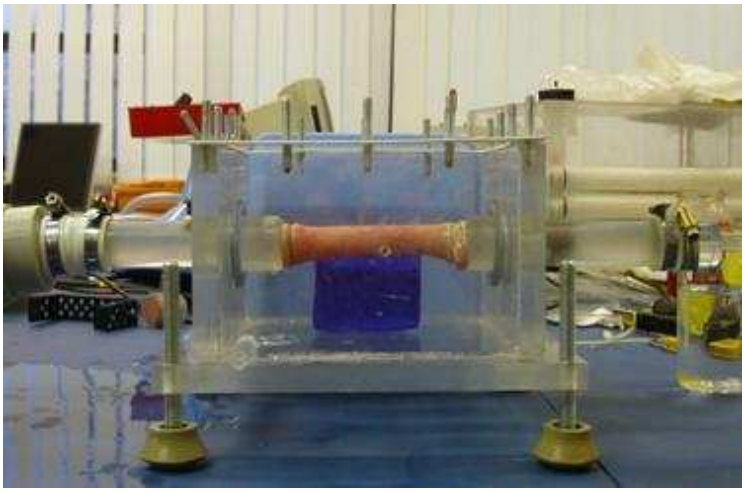

Figure 2: The artery placed into the experimental setup.

the pressurization of the artery required that the remaining holes in the artery be closed. This was performed by inserting a condom into the artery. It is assumed that the mechanical behavior of the whole structure was not significantly influenced by the much thinner and more flexible condom.

4 Results and discussion

Measured morphological data: F47 – thickness in reference state $H = 2.2$ mm; opening angle $\alpha = 75°$, reference outer radius $R^*{}_o = 17.19$ mm; reference inner radius $R^*{}_i = 14.99$ mm, outer radius of the closed but not pressurized artery $r_o = 10.49$ mm; inner radius of the closed but not pressurized artery $r_i = 8.29$ mm –; M54 – thickness in reference state $H = 2.04$ mm; opening angle $\alpha = 83°$, reference outer radius $R^*{}_o = 19.33$ mm; reference inner radius $R^*{}_i = 17.29$ mm, outer radius of the closed but not pressurized artery $r_o = 10.88$ mm; inner radius of the closed but not pressurized artery $r_i = 8.84$ mm.
The inflation tests seemed to be reproducible after several pre–cycles. In accordance with the concept of pseudoelasticity, see [16] or [1] and [2], only the loading parts of the inflation tests were included in the regression. The third and fourth cycle for each axial pre–strain, $\lambda_z = 1.32$ and 1.4, were selected for identification of the material parameters in the case of F47, and the four and sixth cycle upon axial pre-strains $\lambda_z = 1.3$ and first and third upon $\lambda_z = 1.42$ in the case of M54. The adjustment of the experimental data is shown in Figure 3. The systems of nonlinear regression equations (13) were solved by the Levenberg – Marquardt method. Estimated values of the material parameters are shown in Table 1. The fitted models achieved values of the determination coefficient of $I^2 = 0.96$ in the case of F47, and $I^2 = 0.97$ in the case of M54. The material model of the combined strain energy density function (1) fits the experimental data of the inflated and elongated aorta very well. Unfortunately, to the best knowledge of the authors there is no available data in the literature about the mechanical response of a human

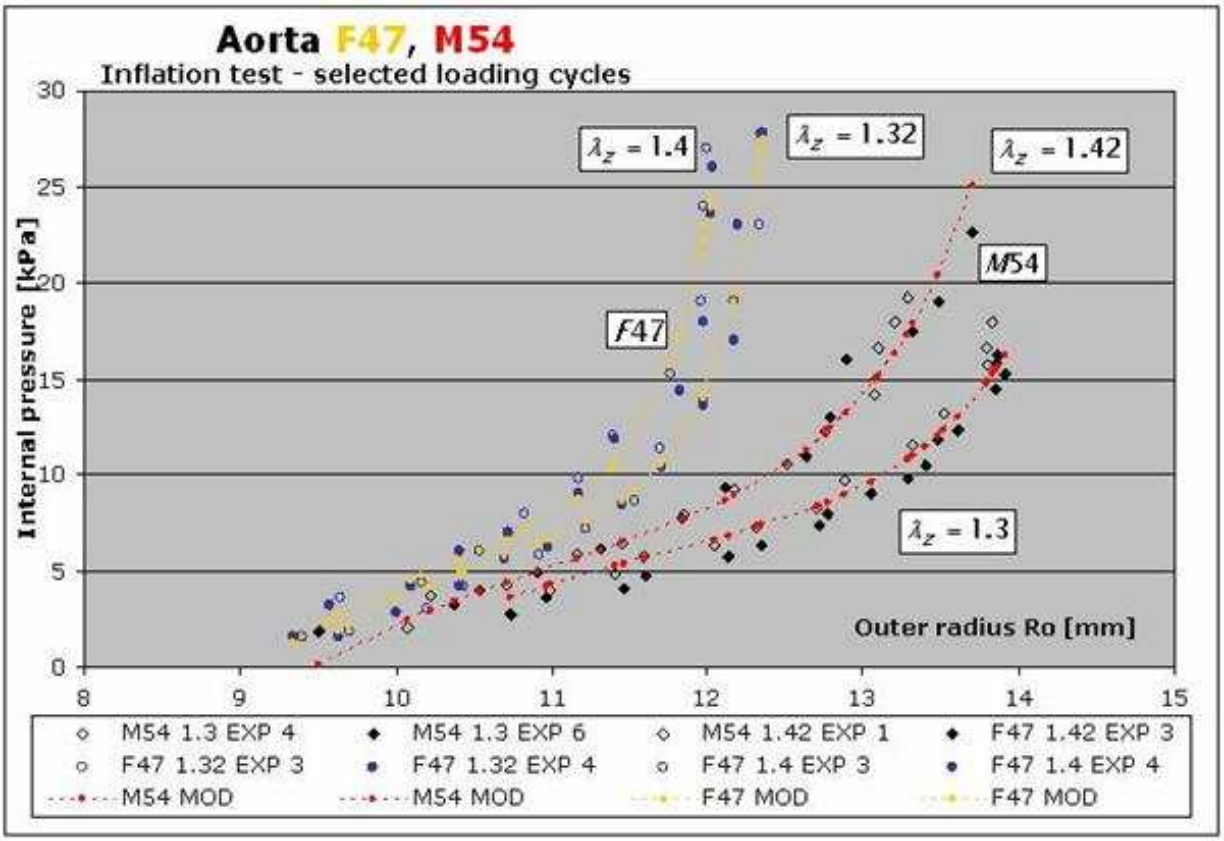

Figure 3: Adjustment of experimental data. The table placed below the diagram summarizes the data as follows: M54 1.3 EXP 4 – aorta M54; $\lambda_z = 1.3$; experimental point; fourth cycle; F47 MOD – aorta F47; fitted model point.

aorta governed by model (1) for a direct comparison. However, it is well known that biological tissues show large individual differences, so that any comparison could be problematic. However, if we compare the material parameters in Table 1 with [12], we can conclude that they exhibit stress–like parameters of the same order.

The legend to Figure 3 is shown below the figure. Note that the observation points are displayed as full or empty circles and diamonds. The blue circles refer to the F47 artery, while the black diamonds refer to M54. The full and empty signs distinguish different loading cycles. The material of the arterial walls exhibits significant stiffening under large strains. The typical S–shape of the pressure – radius curve is shown. Note the good agreement between the measured data and the model in the low pressure domain, because model (1) was proposed with the aim of achieving better results here, see the papers published by the authors of combination (1) in [11], [12] and in section 4 in [19] and [20]. In [20], we find other values of the material parameters published by Holzapfel, Weizsäcker et al, related to a rat aorta.

The material parameters related to meaningful deformation states could not be selected arbitrarily. We would like to point out that the estimated material parameters in Table 1 satisfy the convexity conditions. They are positive and satisfy the relation:

$$4b_1\, b_2 - b_3^2 > 0 \tag{14}$$

A general discussion of material models for arterial walls is available in [2], and there is a discussion of model (1) in [10].

5 Conclusion

The inflation–extension tests of a human thoracic aorta presented here were performed with the aim of fitting the material model. The computational model of a thick–walled tube with axial pre–strains was used to obtain a suitable equation for nonlinear regression. The residual strains in the circumferential direction were included. The passive mechanical response of an artery was governed by a combined model of the strain energy density function (1). This combined model includes an isotropic Neo–Hookean expression related to the low strain response and a Fung–type expression related to large strains and the anisotropy of the wall. Hence, the artery was modeled as an incompressible, orthotropic and nonlinear hyperelastic homogeneous continuum. The nonlinear regression was based on the boundary condition of a pressurized thick–walled tube at the inner radius. The experimentally measured data were compared with the prediction of the model. The standard least squares method was used to estimate the material parameters. The numerical values of the parameters were obtained by solving nonlinear regression equations by the Levenberg–Marquardt method.
A typical S–shaped pressure–radius relation was found in both specimens. The pressure – radius curve is nonlinear, with significant stiffening under large strains. The plotted experimental data and the model predictions display good agreement. This is supported by the values of the determination coefficient $I^2 = 0.96 - 0.97$. The identified material parameters satisfy the convexity conditions, and have positive values. Hence, we can conclude that material model (1) with the parameters from Table 1 is a suitable material model for the passive arterial response to mechanical loads.

Acknowledgement

This research has been gratefully supported by Czech Science Foundation GA CR 106/04/1181 and Czech Ministry of Education, Youth and Sports MSM 68 40 77 00 12.

References

[1] Y. C. Fung, K. Fronek, and P. Patitucci. Pseudoelasticity of arteries and the choice of its mathematical expression. American Journal of Physiology, 237:H620–H631, 1979.

[2] G. A. Holzapfel, T. C. Gasser, and R. W. Ogden. A new constitutive framework for arterial wall mechanics and a comparative study of material models. Journal of Elasticity, 61:1–48, 2000.

[3] T. C. Gasser, R. W. Ogden, and G. A. Holzapfel. Hyperelastic modeling of arterial layers with distributed collagen fiber orientations. Journal of the Royal Society Interface, 3:15–35, 2005.

[4] M. A. Zulliger, P. Fridez, K. Hayashi, N. Sterigopulos. A strain energy density function for arteries accounting for wall composition and structure. Journal of Biomechanics, 37:989–1000, 2004.

[5] H. Demiray, and R. P. Vito. A layered cylindrical shell model for an aorta. International Journal of Engineering Science, 29:47–54, 1991.

[6] W. W. von Maltzahn, D. Besdo, and W. Wiemer. Elastic properties of arteries: A nonlinear two-layer cylindrical model. Journal of Biomechanics, 14:389-397, 1981.

[7] A. Rachev. Theoretical study of the effect of stress-dependent remodeling on arterial geometry under hypertensive conditions. Journal of Biomechanics, 30:819–827, 1997.

[8] N. J. B. Driessen, C. V. C. Bouten and F. P. T. Baaijens. A Structural Constitutive Model For Collagenous Cardiovascular Tissues Incorporating the Angular Fiber Distribution. Journal of Biomechanical Engineering, 127:494–503, 2005.

[9] G. A. Holzapfel, T. C. Gasser, and R. W. Ogden. Comparison of a Multi-layer Structural Model for Arterial Walls with a Fung-Type Model, and Issues of Material Stability. Journal of Biomechanical Engineering, 126:264-275, 2004.

[10] G. A. Holzapfel. Determination of material models for arterial walls from uniaxial extension tests and histological structure. Journal of Theoretical Biology, 238:290-302, 2006.

[11] H. W. Weizsäcker, et al. Strain energy density function for arteries from different topographical sites. *Biomed. Technik.*, 40:139–141, 1995.

[12] G. A. Holzapfel, and H. W. Weizsäcker. Biomechanical behavior of the arterial wall and its numerical characterization. Computers in Biology and Medicine, 28**:**377–392, 1998.

[13] M. Carboni, G. W. Desch, and H. W. Weizsäcker. Passive mechanical properties of porcine left circumflex artery and its mathematical description. Medical Engineering and Physics, in press.

[14] C. A. J. Schulze-Bauer, C. Mörth, and G. A. Holzapfel. Passive Biaxial Mechanical Response of Aged Human Iliac Arteries. Journal of Biomechanical Engineering, 125:395-406, 2003.

[15] M. R. Roach, and A. C. Burton. The reason for the shape of the distensibility curve of arteries. Canadian Journal of Biochemistry and Physiology, 35:681-690, 1957.

[16] K. Hayashi. Mechanical Properties of Soft Tissues and Arterial Walls. In G. A. Holzapfel and R. W. Ogden, editors, Biomechanics of soft tissue in cardiovascular systems. Springer, Vienna, 2003.

[17] A. Rachev, and S. E. Greenwald. Residual strains in conduit arteries. Journal of Biomechanics, 36:661-670, 2003.

[18] T. Matsumoto, and K. Hayashi. Stress and Strain Distribution in Hypertensive and Normotensive Rat Aorta Considering Residual strain. Journal of Biomechanical Engineering, 118:62-73, 1996.

[19] G. A. Holzapfel, R. Eberlein, P. Wriggers, and H. W. Weizsäcker. Large strains analysis of soft biological membranes: Formulation and finite element analysis. Computer methods in applied mechanics and engineering, 132:45-61, 1996.

[20] G. A. Holzapfel, R. Eberlein, P. Wriggers, and H. W. Weizsäcker. A new axisymmetrical membrane element for anisotropic, finite strain analysis of arteries. Communications in numerical methods in engineering, 12:507-517, 1996.

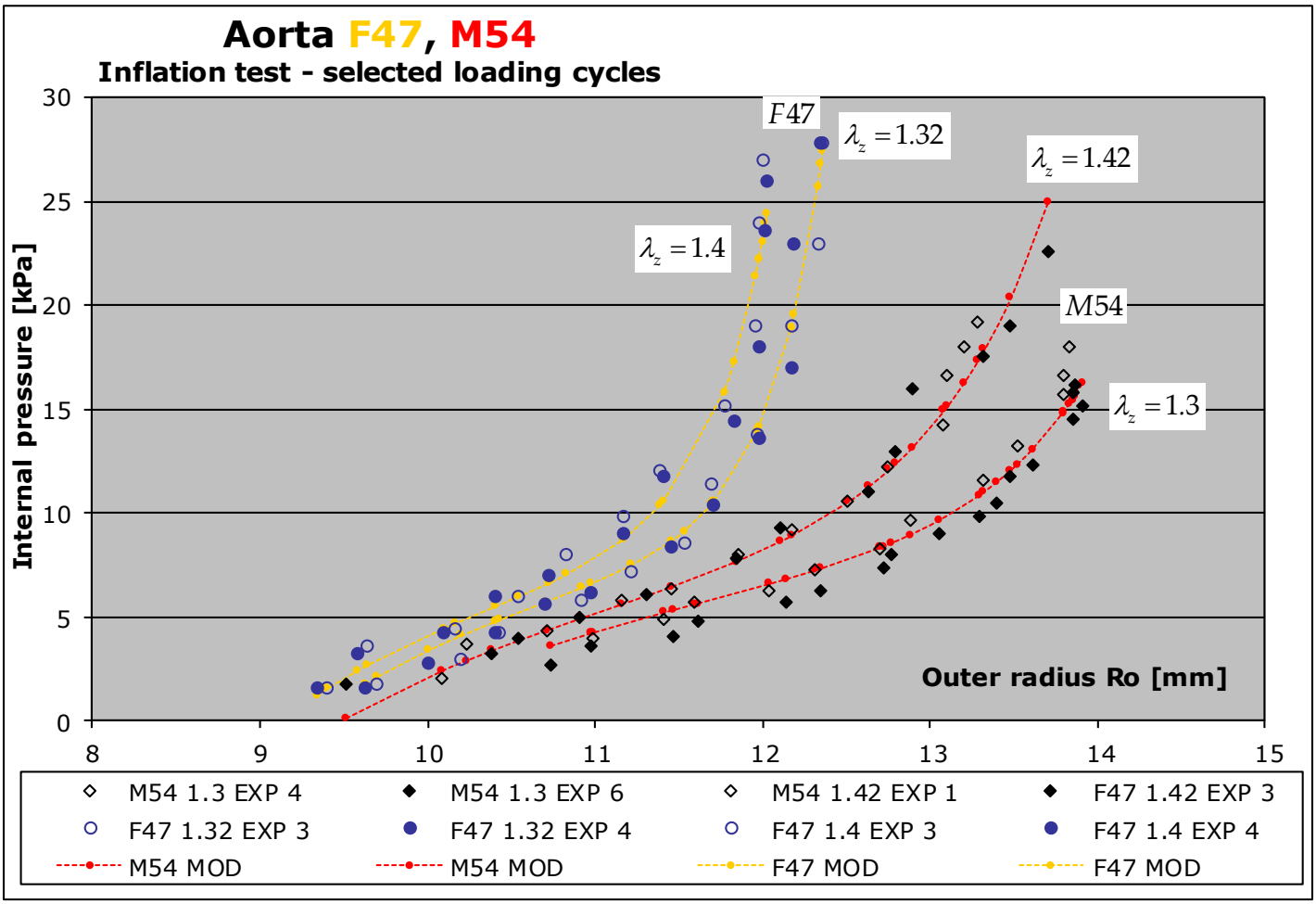
Aorta F47, M54
Inflation test - selected loading cycles
Internal pressure [kPa]
Outer radius Ro [mm]
F47
$\lambda_z = 1.32$
$\lambda_z = 1.42$
$\lambda_z = 1.4$
M54
$\lambda_z = 1.3$
0
5
10
15
20
25
30
8
9
10
11
12
13
14
15
M54 1.3 EXP 4
M54 1.3 EXP 6
M54 1.42 EXP 1
F47 1.42 EXP 3
F47 1.32 EXP 3
F47 1.32 EXP 4
F47 1.4 EXP 3
F47 1.4 EXP 4
M54 MOD
M54 MOD
F47 MOD
F47 MOD